Telomere dysfunction and evolution of intestinal carcinoma in mice and humans

Karl Lenhard Rudolph[1,4], Melissa Millard[1], Marcus W. Bosenberg[1,2] & Ronald A. DePinho[1,3]

Telomerase activation is a common feature of advanced human cancers[1] and facilitates the malignant transformation of cultured human cells[2] and in mice[3,4]. These experimental observations are in accord with the presence of robust telomerase activity in more advanced stages of human colorectal carcinogenesis[5–7]. However, the occurrence of colon carcinomas in telomerase RNA (*Terc*)-null, p53-mutant mice[8] has revealed complex interactions between telomere dynamics, checkpoint responses and carcinogenesis9. We therefore sought to determine whether telomere dysfunction exerts differential effects on cancer initiation versus progression of mouse and human intestinal neoplasia. In successive generations of *Apc*^{Min} *Terc*$^{-/-}$ mice[10,11], progressive telomere dysfunction led to an increase in initiated lesions (microscopic adenomas), yet a significant decline in the multiplicity and size of macroscopic adenomas. That telomere dysfunction also contributes to human colorectal carcinogenesis is supported by the appearance of anaphase bridges (a correlate of telomere dysfunction) at the adenoma-early carcinoma transition, a transition recognized for marked chromosomal instability[12–15]. Together, these data are consistent with a model in which telomere dysfunction promotes the chromosomal instability that drives early carcinogenesis, while telomerase activation restores genomic stability to a level permissive for tumor progression. We propose that early and transient telomere dysfunction is a major mechanism underlying chromosomal instability of human cancer.

Epithelial cancers occur infrequently in laboratory mice, and when they do occur they rarely exhibit the aberrant cytogenetic profiles typical of human carcinomas, such as severe aneuploidy and complex nonreciprocal translocations[8,16]. The long telomeres and somatic expression of telomerase in mice would seem to contribute to these species differences as evidenced by the emergence of epithelial cancers with chromosomal instability in telomerase-deficient, p53-mutant mice with short dysfunctional telomeres[8]. To delineate the complex role of telomere dysfunction in the initiation and progression of intestinal carcinoma, we monitored the impact of increasing levels of telomere dysfunction on the rate, growth and clinical behavior of gastrointestinal neoplasias in *Apc*^{Min} mice. In this model, loss of the wildtype *Apc* allele causes multiple intestinal neoplasia (Min) in 100% of *Apc*^{Min} mice and death at 4–6 months[10,11]. The quantitative nature of the adenoma phenotype allows us to examine tumor initiation as well as progression from micro- to macroadenoma.

To avoid strain-specific modification of the *Apc*^{Min} phenotype[17,18], we backcrossed the *Terc*$^{-/-}$ allele to C57BL/6 (B6) mice (N7) and then mated the mice with congenic B6 *Apc*^{Min} mice. B6 mice possess shorter telomere lengths (on average) than the mixed genetic strains studied previously[19–22], which produces an onset of chromosomal instability in the second generation (G2) *Terc*$^{-/-}$ mice and a marked increase in chromosomal aberrations in G3 and G4 mice. Although survival curves of *Terc*$^{+/+}$ *Apc*^{Min} and G1 *Terc*$^{-/-}$ *Apc*^{Min} mice are superimposable, we observed a decrease in survival in G2 and G3 *Terc*$^{-/-}$ *Apc*^{Min} mice, whereas G4 *Terc*$^{-/-}$ *Apc*^{Min} mice show a marked increase in survival (Fig. 1). These complex survival trends indicate that the level of telomere dysfunction may differentially influence the emergence and the subsequent growth of adenomas.

To assess more directly telomere-related effects on initiation versus progression of *Apc*^{Min} neoplasias, we quantitated microadenomas and macroadenomas in whole-mount intestinal preparations derived from the various *Terc*$^{-/-}$ generations (Fig. 2). The range and average number of microadenomas are similar in *Terc*$^{+/+}$ and G1 *Terc*$^{-/-}$ *Apc*^{Min} mice, compared with a significant increase in microadenoma formation in G3 and G4 *mTerc*$^{-/-}$ *Apc*^{Min} samples (Fig. 2*a*). In contrast to the microadenoma trend, macroadenoma formation peaks modestly in G2 *Terc*$^{-/-}$ *Apc*^{Min} mice but declines in G3 and significantly in G4 *Terc*$^{-/-}$ *Apc*^{Min} mice (Fig. 2*b*). One G3 and five of six G4 *Terc*$^{-/-}$ *Apc*^{Min} mice showed near-complete suppression of macroadenoma formation and markedly impaired adenoma growth (Figs. 2*b*, 3*a*). Macroadenoma burden correlates inversely with survival trends across the *Apc*^{Min} *Terc*$^{-/-}$ generations (Fig. 1). Finally, the ratio of micro- to macroadenoma formation in these

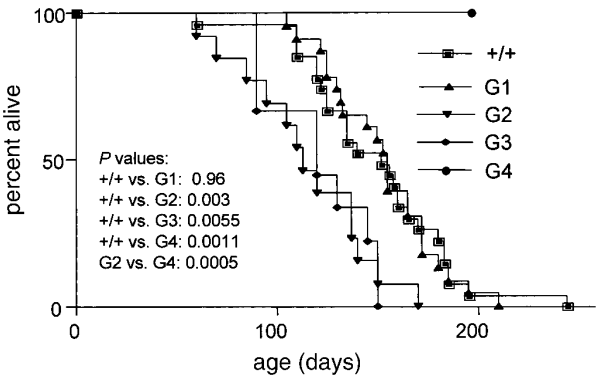

Fig. 1 Telomere shortening has contrasting effects on the survival of *Apc*^{Min} mice. We examined survival of the B6 *Apc*^{Min} in *Terc*$^{+/+}$ and *Terc*$^{+/-}$ mice (adequate telomere function, positive telomerase activity), G1 *Terc*$^{-/-}$ mice (adequate telomere function, no telomerase activity), G2 *Terc*$^{-/-}$ mice (moderate telomere dysfunction, no telomerase activity) and G3–G4 *Terc*$^{-/-}$ mice (severe telomere dysfunction, no telomerase). Survival in *Terc*$^{+/+}$ was no different than survival in G1 *Terc*$^{-/-}$ mice. A significant decrease in survival was noted in mid-generation (G3 and G2 *Terc*$^{-/-}$) mice. In contrast, we observed a significant increase in the lifespan in late-generation (G4) *Terc*$^{-/-}$ mice. Note that 7 months after birth none of the G4 *Terc*$^{-/-}$ mice had died and that animals were sacrificed at that time to analyze the tumor burden.

[1]*Department of Adult Oncology, Dana-Farber Cancer Institute, Boston, Massachusetts 02115, USA.* [2]*Department of Pathology, Brigham and Women's Hospital, Boston, Massachusetts 02115, USA.* [3]*Departments of Medicine and Genetics, Harvard Medical School, Boston, Massachusetts 02115, USA.* [4]*Department of Gastroenterology and Hepatology, Medical School Hannover, Hannover 30623, Germany. Correspondence should be addressed to R.A.D. (e-mail: ron_depinho@dfci.harvard.edu).*

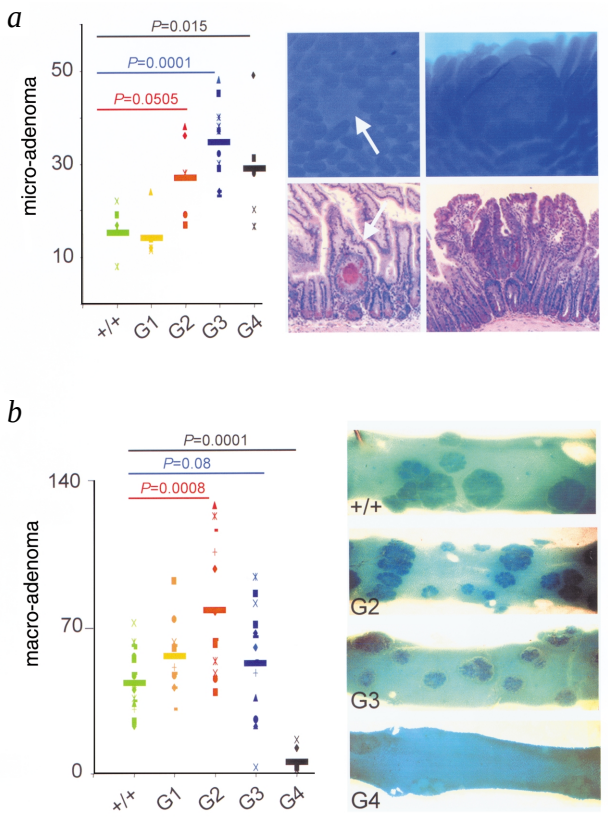

Fig. 2 Contrasting effects of telomere shortening on tumor formation in Apc^{Min} mice. We determined the number of micro- and macroadenomas in $Terc^{+/+}$ and G1–G4 $Terc^{-/-}$ mice carrying the Apc^{Min} mutation. The age of the mice ranged from 3.5 to 5 months at the time of the analyses; only G4 mice were characterized at 7 months of age due to the increased lifespan. ***a***, Whereas the number of microadenomas was no different in G1 $Terc^{-/-}$ than in $Terc^{+/+}$ mice, we observed a twofold increase in the number of microadenomas in G2–G4 $Terc^{-/-}$ mice. Photomicrographs show representative examples of the morphological (whole-mount, top) and histological (bottom) appearance of cystic crypts (left) and microadenomas (right). ***b***, A significant increase in the number of macroadenomas is present only in G2 $Terc^{-/-}$ mice compared with $mTerc^{+/+}$ mice. In contrast, the number of macroadenomas decreases in G3 $Terc^{-/-}$ mice and is markedly suppressed in G4 $Terc^{-/-}$ mice. In general, the number of macroadenomas correlates inversely to Apc^{Min} survival trends (Fig. 1). Photomicrographs on the right show representative examples of the appearance of macroadenomas in the terminal ileum of the different generations indicated (magnification, ×7.5).

different generations further substantiates the adverse effect of telomere dysfunction on intestinal tumor progression (Fig. 3*b*). Thus, Apc^{Min} adenoma growth and progression are suppressed significantly in late $Terc^{-/-}$ generations, despite an increased incidence of initiated neoplastic lesions.

In the evaluation of the molecular events modulating the Apc^{Min} phenotype, polymerase chain reaction (PCR)-based allelotyping of G2–G4 $Terc^{-/-}$ Apc^{Min} adenomas shows wildtype *Apc* allele loss in 90% of microadenomas (n=10), 100% of macroadenomas (n=21) and none of the non-tumor-bearing intestinal mucosal biopsies from late-generation $Terc^{-/-}$ Apc^{Min} mice (n=6) (data not shown). The main mechanism of *Apc* loss in Apc^{Min} mice involves loss of the entire chromosome 18 carrying the wildtype *Apc* allele followed by duplication of the remaining chromosome carrying the mutant allele[23]. Mitotic recombination is a second possible mechanism and has been identified as a cause of *Apc* loss in Bloom-deficient Apc^{Min} mice[24]. It is reasonable to assume that chromosomal loss is enhanced in the setting of telomere dysfunction through the formation of dicentric chromosomes and their high rate of loss[3,8]. In line with this hypothesis, the very low anaphase bridge index[25–28] (ABI) of $Terc^{+/+}$ and G1 $Terc^{-/-}$ Apc^{Min} adenomas contrasted sharply with a higher than normal ABI in the adenomas of later $Terc^{-/-}$ generations (Fig. 4*a*).

Fig. 3 Telomere shortening inhibits progression of intestinal neoplasia. The size of macroadenomas and the ratio of micro- to macroadenomas were determined in $Terc^{+/+}$ and G1–G4 $Terc^{-/-}$ mice carrying the Apc^{Min} mutation. ***a***, We first observed a significant decrease in the size of macroadenomas in G2 $Terc^{-/-}$ mice compared with $Terc^{+/+}$ mice. G4 $Terc^{-/-}$ mice show a further decrease in macroadenoma size. Right, representative examples of the histological appearance of the macroadenoma size difference in G1 and G3 $Terc^{-/-}$ mice (magnification for both samples, ×100). ***b***, Ratio of micro- to macroadenomas determined in individual $Terc^{+/+}$ and G1–G4 $Terc^{-/-}$ mice.

Checkpoint responses that are dependent on p53 underlie the adverse cellular consequences of telomere dysfunction[29,30]. To determine whether such mechanisms contribute to impaired progression of late generation $Terc^{-/-}$ Apc^{Min} adenomas, we determined p53 status and expression as well as intratumoral rates of apoptosis and cell proliferation in adenoma samples from the different cohorts. All macroadenomas and matched normal mucosal biopsies tested by a PCR-based assay retained both copies of the *Trp53* allele (Fig. 4*b*). In addition, we detected overexpression of p53 by immunofluorescence in G3 $Terc^{-/-}$ adenomas, which is more pronounced in G4 $Terc^{-/-}$ adenomas (Fig. 4*c*). Correspondingly, we detected increased apoptosis and decreased proliferation in G3 and G4 $Terc^{-/-}$ adenomas, with near complete suppression of proliferation in G4 $Terc^{-/-}$ adenomas (Fig. 4*d*,*e*). Thus, the basis for impaired progression in G3 and G4 $Terc^{-/-}$ adenomas is probably due to checkpoint responses activated in the setting of anaphase bridge breakage and intact DNA-damage responses and may be compounded by the rampant genomic instability induced by advanced telomere dysfunction[3,4,8,29].

Do these findings in the mouse provide a framework for understanding telomere-dependent mechanisms in human carcinoma development? If telomeres were to modulate the malignant

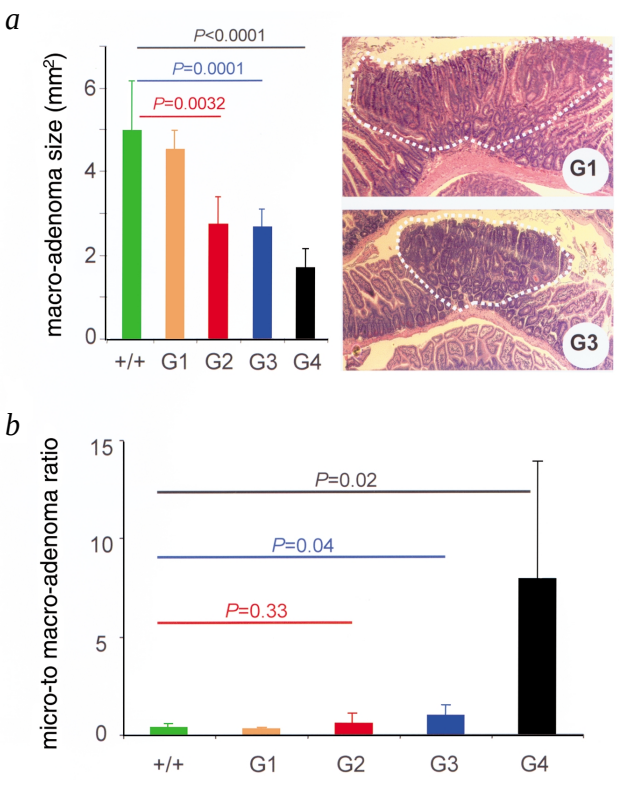

process in humans, one would anticipate their greatest impact to be at the point of maximal attrition just before, or at the time of, telomerase activation. In this regard, it is notable that chromosomal instability (of the type associated with, but not specific for, telomere dysfunction) increases markedly at the transition from late adenomatous polyps to carcinomas. Moreover, p53 function, a potent barrier for 'aspiring' cancer cells with telomere dysfunction, is often lost in these emerging carcinomas[16]. Lastly, telomerase is reactivated late in the evolution of colorectal carcinoma, a pattern that correlates well with telomere attrition. The confluence of these events in humans and in the mouse data presented here and reported previously[8,22,29] leads us to propose that telomere dysfunction is a key mechanism driving chromosomal instability at the benign-to-malignant transition in human colorectal carcinogenesis, thereby enabling premalignant cells to reach a critical cancer threshold[9]. If this process is operative, then a hallmark of telomere dysfunction, anaphase bridge formation, should be evident as adenomatous lesions assume high-grade dysplastic features.

To test this hypothesis, we determined the ABI for sporadic human colorectal tumor samples representing different stages of tumor progression: adenoma, adenoma with high-grade dysplasia, adenocarcinoma arising in an adenomatous polyp (carcinoma-in situ), primary adenocarcinoma, and metastasis (Fig. 5). The ABI is very low in early adenomas but increases sharply in foci of high-grade dysplasia and CIS (Fig. 5a). We observed a further, but not significant, increase in deeply invasive primary adenocarcinoma, whereas metastasis show a significant reduction in the ABI compared with primary adenocarcinoma. Together, the presence of short telomeres in colorectal carcinoma[5,31], the activation of telomerase at the carcinoma stage[5–7], the sharp increase of anaphase bridges at the adenoma–carcinoma transition and the decrease of anaphase bridges in metastasis imply that telomere dynamics contribute to the known genomic and phenotypic characteristics of human colorectal carcinoma progression. Given the prominent role of chromosomal instability in human colorectal cancer initiation and the strong selection of telomerase-expressing cells later during cancer progression, the telomerase-deficient Apc^{Min} mouse provides a system in which to model this critical stage in the life history of a colorectal cancer cell.

Methods

Terc Apc^{Min} mouse. We backcrossed $Terc^{+/-}$ mice of a mixed genetic background[21] to C57BL6J mice for seven generations before we performed crosses to C57BL6J Apc^{Min} mice. Intercrosses of $Terc^{+/-}$ Apc^{Min} mice according to previously published mating schemes[19] results in successive generations of $Terc^{-/-}$ Apc^{Min} mice ($Terc^{+/+}$ and G1–G4 $mTerc^{-/-}$). Segregation studies reveal similar transmission for the mutant Apc^{Min} allele in all *Terc* generations (39% in $Terc^{+/+}$ and G1 $Terc^{-/-}$, 41% in G2 and G3 $Terc^{-/-}$ and 38% in G4 $Terc^{-/-}$).

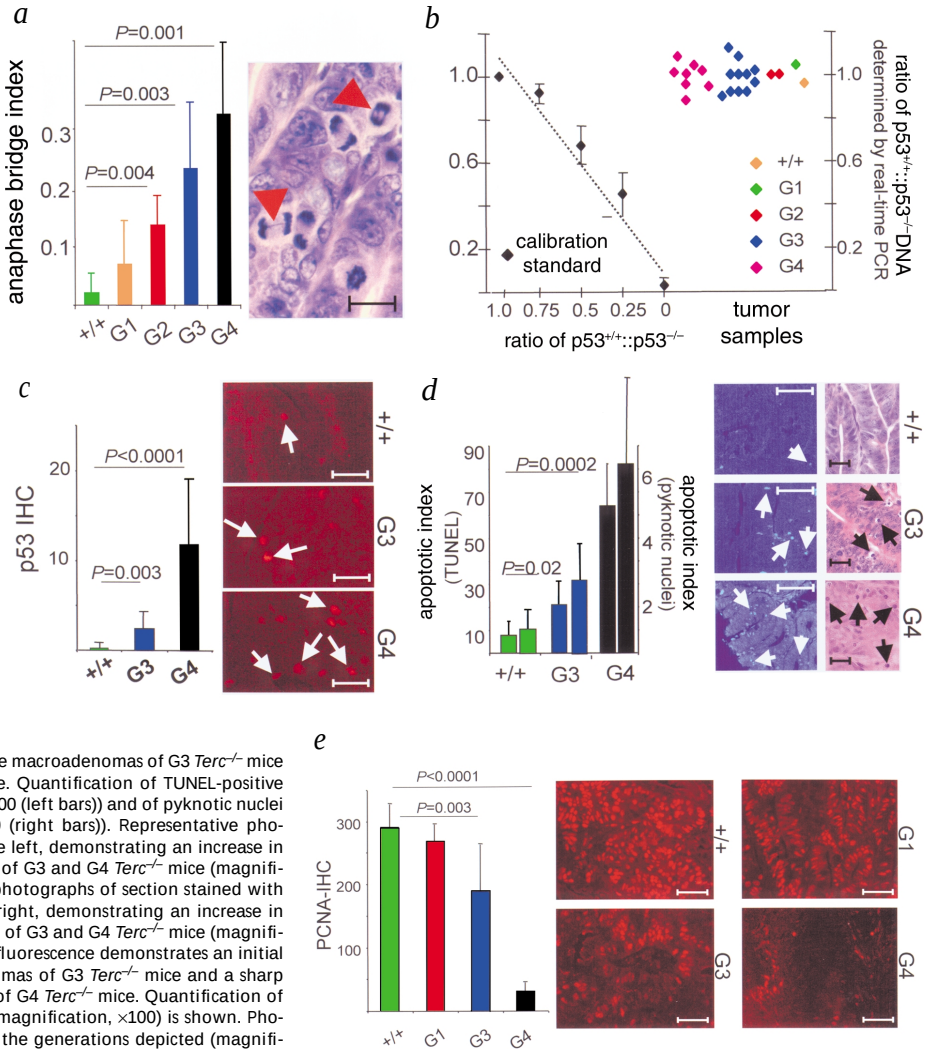

Fig. 4 Degree of telomere dysfunction affects adenoma progression. ***a***, We determined the ABI in the macroadenomas of $Terc^{+/+}$ and G1–G4 $Terc^{-/-}$ mice by calculating the ratio of anaphase bridges to normal appearing anaphases. A significant increase in anaphase bridges appears first in G2 $Terc^{-/-}$ mice and a further significant increase is evident in G4 $Terc^{-/-}$ mice. Right, example of two anaphase bridges (arrows) and two normal appearing anaphases (magnification, ×1,000; bar, 30 μm). ***b***,***c***, Retention and overexpression of p53 in macroadenomas of $Terc^{-/-}$ Apc^{Min} mice. *Trp53* gene dosage was quantified by real-time PCR with a Molecular Beacons assay (***b***). The standard curve was calculated on mixtures of DNA derived from the intestines of $Trp53^{-/-}$ and $Trp53^{+/+}$ mice with the ratios indicated. No significant decrease in signal intensity is detected in 23 macroadenomas investigated from $Terc^{+/+}$ and G1–G4 $Terc^{-/-}$ Apc^{Min} mice. Immunofluorescence of p53 reveals overexpression of p53 in adenomas arising in G3 and G4 $Terc^{-/-}$ mice (***c***). Histogram represents quantification of p53-positive nuclei per high-power field (magnification, ×400). Right, representative immunofluorescent stains from $Terc^{+/+}$ and G3–G4 $Terc^{-/-}$ adenomas (magnification, ×400; bar, 50 μm). ***d***, We observed an increased number of apoptotic cells in the macroadenomas of G3 $Terc^{-/-}$ mice that is more pronounced in G4 $Terc^{-/-}$ mice. Quantification of TUNEL-positive cells per low-power field (magnification, ×100 (left bars)) and of pyknotic nuclei per high-power field (magnification, ×400 (right bars)). Representative photographs of TUNEL assays are shown on the left, demonstrating an increase in apoptotic cells (arrows) in macroadenomas of G3 and G4 $Terc^{-/-}$ mice (magnification, ×100; bar, 150 μm); representative photographs of section stained with hematoxylin and eosin are shown on the right, demonstrating an increase in pyknotic nuclei (arrows) in macroadenomas of G3 and G4 $Terc^{-/-}$ mice (magnification, ×200; bar, 50 μm). ***e***, PCNA immunofluorescence demonstrates an initial decrease in proliferating cells in the adenomas of G3 $Terc^{-/-}$ mice and a sharp decrease in proliferation in the adenomas of G4 $Terc^{-/-}$ mice. Quantification of PCNA-positive nuclei per low-power field (magnification, ×100) is shown. Photographs show representative examples of the generations depicted (magnification, ×200; bar, 100 μm).

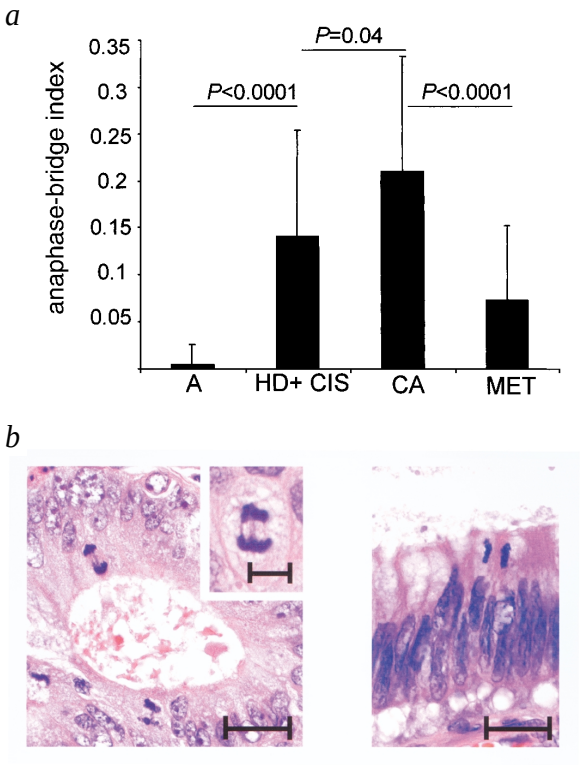

Fig. 5 Telomere dysfunction peaks at the adenoma-carcinoma transition in human colorectal carcinogenesis. ***a***, We determined the rate of anaphase bridge formation at different stages of human colorectal carcinogenesis: adenoma (AD; 26 cases), high-grade dysplasia (HD) and adenocarcinoma present in adenomatous polyps (CIS; 24 cases), invasive adenocarcinoma (CA; 33 cases) and metastasis (MET; 29 cases). Ratio of anaphase bridges to total number of anaphases is shown. Photographs show representative examples of anaphase bridges in a carcinoma specimen (***b***) and a normal anaphase in an adenoma (***c***) (magnification, ×600; bar, 50 μm; inset magnification, ×1,000; bar, 15 μm).

Survival curves. We monitored the health status of the different cohorts of *Terc Apc*^{Min} mice (16 *Terc*$^{+/+}$, 19 G1, 14 G2, 14 G3 and 6 G4 *mTerc*$^{-/-}$ mice) during weekly inspections of the mouse colony. We used the survival data of mice that were sacrificed because of severely impaired health status and of mice that died between observation rounds to calculate survival curves for the different cohorts.

Whole-mount staining/analysis of micro- and macroadenomas. The complete small and large intestine of the mice was resected *en block*, opened longitudinally and pinned luminal side up on Styrofoam. We counted macroadenomas (1–5 mm diameter) before the whole-mount staining. Whole-mount staining was performed after overnight fixation in 3% formalin in phosphate-buffered saline (PBS) at 4 °C. After a rinse in fresh PBS, the intestines were stained for 3–5 min in 0.2% methylene blue in PBS. After two washes in PBS, the intestines were kept in PBS for an additional 30–60 min with shaking. We quantified the microadenoma counts (<1 mm) on the entire small intestine with a Leica dissecting microscope (magnification, ×7–40). We dissected single microadenomas with a 26-gauge syringe for DNA extraction. Adenoma size in individual mice (n=6 for each cohort) was determined with a dissection microscope (magnification, ×15) and an optical micrometer. For each mouse, we determined the size of 3–15 adenomas located in the last 5 cm of the terminal ileum and calculated mean values.

Histology and immunohistochemistry. We used longitudinal cross sections (5 μm thick) through intestinal rolls spanning the entire small intestine for histological and immunohistochemical analyses. We used sections stained with hematoxylin and eosin to compare histological morphology and to quantify anaphase bridges and pyknotic nuclei. Unstained sections were stained for apoptotic cells with the fluorescent cell death detection kit (Roche). A 1:200 dilution of the p53-Ab-1 antibody (Oncogene) was used for immunofluorescence of p53 and a 1:200 dilution of the PCNA-Ab-1 antibody (Oncogene) was used to detect proliferating cell nuclear antigen (PCNA). Stained sections were dehydrated and mounted.

Apc analysis. A PCR-based analysis for deletion of the wildtype *Apc* allele was performed as described previously[23]. We used two PCR primers to amplify the *Apc* locus spanning the *Apc*^{Min} point mutation at nucleotide 2549 (forward, 5′–TCTCGTTCTGAGAAAGACAGAAGCT–3′; reverse, 5′–TGATACT TCTTCTTCCAAAGCTTTGGCTAT–3′). Both primers contained *Hin*dIII restriction sides. An additional *Hin*dIII restriction site was present only in the wildtype *Apc* PCR product and missing in the PCR product of the *Apc*^{Min} allele. The PCR products were digested with *Hin*dIII and separated in a 10% denaturing polyacrylamide gel. DNA products were visualized by staining with ethidium bromide. The wildtype *Apc* allele was 123 base pairs (bp), and the *Apc*^{Min} allele was 155 bp. We quantified the staining intensity for both products on duplicates for each sample and used only samples with reproducible results (within 10% deviation) for analysis of the *Apc* status.

p53 Quantitative (Q)-PCR amplification. Genomic DNA was isolated with a Qiagen Dneasy kit (Qiagen; Valencia) and quantified by real-time PCR using a Molecular Beacons assay. PCR amplifications were performed in replicates of 8 in 25 μl reaction mixtures, each containing 50 ng of genomic DNA, 1× Sentinel Q-PCR core reagent (Stratagene) in 4 mM $MgCl_2$ with each primer at 300 nM and the corresponding fluorescent-labeled probe at 400 nM. Primer and probe sequences are available upon request. Amplifications were done on the ABI Prism 7700 (PE Biosystems) under the following conditions: 95 °C for 3 min, 40 cycles of 95 °C for 15 s, 60 °C for 30 s. We determined the relative quantities of *p53* by normalizing the *p53* gene amplification product to that of the single-copy gene *ApoB* and calibrating the results to a DNA sample known to contain a single copy of *p53*.

Human samples. All cases of human colorectal adenomas (n=26), HD and adenocarcinoma arising in adenomatous polyps (n=24), invasive adenocarcinomas (n=33) and metastasis (n=29) were retrieved from the archives of the Department of Pathology, Brigham and Women's Hospital and the Medical School Hannover (Germany). We reviewed the diagnoses and determined the ABI for each morphologically distinct tumor stage present. The ABI was determined by dividing the number of nuclei with anaphase bridges by the total number of anaphase nuclei. Two investigators independently scored a minimum of 10 anaphases per sample. Anaphase bridging was defined as anaphases in which greater than two-thirds of the distance between the separating anaphase poles was spanned by the bridging chromosome to avoid counting lagging chromosomes.

Acknowledgments

We thank D. Castrillon and S. Chang for helpful advice regarding the pathological and histological classification of intestinal neoplasia; L. Chin, S. Weiler and R. Greenberg for critical review of the manuscript; and P. Flemming and M. Manns for access to the histology archives of the Medical School Hannover. K.L.R. was supported by Deutsche Forschungsgemeinschaft grant Ru 745/1-1, M.W.B. is supported by a Howard Hughes Medical Institute Physician Postdoctoral fellowship and the work was supported by National Institutes of Health grants to R.A.D., who is an American Cancer Society Research Professor and a Kirsch Foundation Scholar.

Received 17 April; accepted 27 April 2001.

1. Kim, N.W. *et al*. Specific association of human telomerase activity with immortal cells and cancer. *Science* **266**, 2011–2005 (1994).
2. Hahn, W.C. *et al*. Creation of human tumour cells with defined genetic elements. *Nature* **400**, 464–468 (1999).
3. Greenberg, R.A. *et al*. Short dysfunctional telomeres impair tumorigenesis in the INK4a(delta2/3) cancer-prone mouse. *Cell* **97**, 515–525 (1999).
4. Gonzalez-Suarez, E., Samper, E., Flores, J.M. & Blasco, M.A. Telomerase-deficient mice with short telomeres are resistant to skin tumorigenesis. *Nature Genet*. **26**, 114–117 (2000).
5. Engelhardt, M., Drullinsky, P., Guillem, J. & Moore, MA. Telomerase and telomere length in the development and progression of premalignant lesions to colorectal cancer. *Clin. Cancer Res*. **3**, 1931–1941 (1997).
6. Tang, R., Cheng, A.J., Wang, J.Y. & Wang, T.C. Close correlation between telomerase expression and adenomatous polyp progression in multistep colorectal carcinogenesis. *Cancer Res*. **58**, 4052–4054 (1998).
7. Chadeneau, C., Hay, K., Hirte, H.W., Gallinger, S. & Bacchetti, S. Telomerase activity associated with acquisition of malignancy in human colorectal cancer.

Cancer Res. **55**, 2533–2536 (1995).
8. Artandi, S. *et al*. Telomere dysfunction promotes non-reciprocal translocations and epithelial cancers in mice. *Nature* **406**, 641–645 (2000).
9. Hanahan, D. Benefits of bad telomeres. *Nature* **406**, 573–574 (2000).
10. Moser, A.R., Pitot, H.C. & Dove, W.F. A dominant mutation that predisposes to multiple intestinal neoplasia in the mouse. *Science* **247**, 322–324 (1990).
11. Su, L.K. *et al*. Multiple intestinal neoplasia caused by a mutation in the murine homolog of the APC gene. *Science* **256**, 668–670 (1992).
12. Young, J. *et al*. Genomic instability occurs in colorectal carcinomas but not in adenomas. *Hum. Mutat*. **2**, 351–354 (1993).
13. Okamoto, M. *et al*. Loss of constitutional heterozygosity in colon carcinoma from patients with familial polyposis coli. *Nature* **331**, 273–277 (1988).
14. Ried, T. *et al*. Comparative genomic hybridization reveals a specific pattern of chromosomal gains and losses during the genesis of colorectal tumors. *Genes Chromosom. Cancer* **15**, 234–245 (1996).
15. Meijer, G.A. *et al*. Progression from colorectal adenoma to carcinoma is associated with non-random chromosomal gains as detected by comparative genomic hybridisation. *J. Clin. Pathol*. **51**, 901–909 (1998).
16. Lengauer, C., Kinzler, K.W. & Vogelstein, B. Genetic instabilities in human cancers. *Nature* **396**, 643–649 (1998).
17. Dietrich, W.F. *et al*. Genetic identification of Mom-1, a major modifier locus affecting Min-induced intestinal neoplasia in the mouse. *Cell* **75**, 631–639 (1993).
18. Halberg, R.B. *et al*. Tumorigenesis in the multiple intestinal neoplasia mouse: redundancy of negative regulators and specificity of modifiers. *Proc. Natl. Acad. Sci. USA* **97**, 3461–3466 (2000).
19. Blasco, M.A. *et al*. Telomere shortening and tumor formation by mouse cells lacking telomerase RNA. *Cell* **91**, 25–34 (1997).
20. Herrera, E. *et al*. Disease states associated with telomerase deficiency appear earlier in mice with short telomeres. *EMBO J.* **18**, 2950–2960 (1999).
21. Lee, H.W. *et al*. Essential role of mouse telomerase in highly proliferative organs. *Nature* **392**, 569–574 (1998).
22. Rudolph, K.L. *et al*. Longevity, stress response, and cancer in aging telomerase-deficient mice. *Cell* **96**, 701–712 (1999).
23. Luongo, C. & Dove, W.F. Somatic genetic events linked to the Apc locus in intestinal adenomas of the Min mouse. *Genes Chromosom. Cancer* **17**, 194–198 (1996).
24. Luo, G. *et al*. Cancer predisposition caused by elevated mitotic recombination in bloom mice. *Nature Genet*. **26**, 424–429 (2000).
25. McClintock, B. The stability of broken ends of chromosomes in *Zea mays*. *Genetics* **26**, 234–282 (1941).
26. van Steensel, B., Smogorzewska, A. & de Lange, T. TRF2 protects human telomeres from end-to-end fusions. *Cell* **92**, 401–413 (1998).
27. Kirk, K.E., Harmon, B.P., Reichardt, I.K., Sedat, J.W. & Blackburn, E.H. Block in anaphase chromosome separation caused by a telomerase template mutation. *Science* **275**, 1478–1481 (1997).
28. Rudolph, K.L., Chang, S., Millard, M., Schreiber-Agus, N. & DePinho, R.A. Inhibition of experimental liver cirrhosis in mice by telomerase gene delivery. *Science* **287**, 1253–1258 (2000).
29. Chin, L. *et al*. p53 deficiency rescues the adverse effects of telomere loss and cooperates with telomere dysfunction to accelerate carcinogenesis. *Cell* **97**, 527–538 (1999).
30. Karlseder, J., Broccoli, D., Dai, Y., Hardy, S. & de Lange, T. p53- and ATM-dependent apoptosis induced by telomeres lacking TRF2. *Science* **283**, 1321–1325 (1999).
31. Hastie, N.D. *et al*. Telomere reduction in human colorectal carcinoma and with ageing. *Nature* **346**, 866–868 (1990).